Simulation Approaches for the Study of the Oil Flow Rate Distribution in Lubricating Systems with Rotating Shafts

International Journal of Thermofluids 24 (2024) 100904

Contents lists available at ScienceDirect

International Journal of Thermofluids

journal homepage: www.sciencedirect.com/journal/international-journal-of-thermofluids

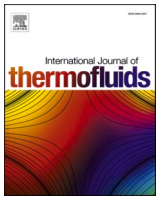

Simulation approaches for the study of the oil flow rate distribution in lubricating systems with rotating shafts

Massimo Rundo [a,*], Paola Fresia [a], Paolo Casoli [b]

[a] Politecnico di Torino, Department of Energy, 10129, Turin, Italy
[b] University of Parma, Department of Engineering for Industrial Systems and Technologies, 43124, Parma, Italy

ARTICLE INFO

Keywords:
CFD
Flow distribution
Lubricating circuit
Rotating pipes

ABSTRACT

This study addresses the issue of predicting the distribution of lubricant flow through the outlets of a rotating shaft used in vehicle power transmission. A typical geometry with closely spaced rows of holes, suitable for the lubrication of multi-disk clutches, was considered. Both lumped parameter and computational fluid dynamics approaches were applied and compared. The test rig for model validation was designed with a variable speed shaft featuring an axial oil inlet and three equally spaced pairs of radial outlet holes. The main characteristic of the experimental facility is the possibility to selectively measure the flow rates through each outlet. It was found that the three-dimensional model based on the multiple reference frame approach provides a reliable prediction of how the flow rate is distributed. Generally, the flow rate is lower through the outlet closest to the inlet and is maximum at the farthest exit. The flow distribution is minimally affected by the shaft speed. The influence of geometric parameters on making the flow distribution more uniform was studied. It was found that a better flow balance is obtained with a low ratio between the diameter of the radial holes and that of the axial channel. The results obtained offer best-practice guidelines for accurately simulating comparable systems, in order to optimize reliability of the mechanical transmission and energy efficiency of the flow generation unit.

1. Introduction

Lubrication is essential in many types of machinery for power transmission. Typical examples are off-road and special vehicles, whether they are equipped with mechanical, hydrostatic, or hybrid transmissions, for traction as well as with Power Take-Off (PTO) for driving auxiliary working hydraulics. The most important function of the lubrication circuit is the reduction of friction between rotating parts for increasing the operating life and for improving the machine's efficiency. Moreover, the lubricant also behaves as coolant medium since a continuous flow of oil at controlled temperature is generated by a feed pump. Typical components to be lubricated are journal and roller bearings, transmission gears as well as clutch disks. For reaching each final oil user, a net of channels is drilled inside the machinery housing and the shafts. For constraint reasons, the use of flow control valves, such as flow dividers, is limited to large portions of the circuit, while the flow rate through each single outlet is controlled only by the hydraulic resistances in the net. Since two or more outlets can be connected in parallel at different distances from the inlet, a significant unbalance of the flow rate could occur with the risk of insufficient lubrication of some mechanical parts. Moreover, if the lubricant flows in a rotating shaft, the centrifugal force acting on the radial ducts generates a kind of suction effect that decreases the pressure in the entire circuit with the risk of air release, being the working pressure of such systems quite low. Since the experimental verification of the actual flow rate through each outlet is typically impossible, it is essential to rely on a suitable simulation tool during the design phase for the appropriate sizing of the circuit, ensuring the correct value of the flow rate for each component, without excessive pressurization that would result in undue energy consumption.

The issue of achieving a uniform flow through parallel paths is much more general. Typical examples are heat exchangers [1,2]. Regarding simulating fluid flow through fixed crossing pipes, such as in hydraulic manifolds, a review of the methodologies can be found in [3]. Additionally, reference [4] provides a comparison between semi-empirical and Computational Fluid Dynamics (CFD) approaches for the evaluating pressure drops. The three-dimensional CFD analysis of the flow through X-shaped junctions for assessing the influence of the crossing angle and the Reynold number using the finite element method is reported in [5]. A software platform in Isight® involving an ANSYS Fluent® module for optimizing the flow of a pipe network with 6 outlets is described in [6]. In this study, hexahedral and wedge/hexahedral

* Corresponding author.
E-mail address: massimo.rundo@polito.it (M. Rundo).

https://doi.org/10.1016/j.ijft.2024.100904

Available online 5 October 2024

Nomenclature

Symbols

A	flow area
A'	dimensionless parameter function of the flow rates
C_d	discharge coefficient
D_C	diameter of the axial channel
D_R	diameter of the radial ducts
Q_{in}	ingoing volumetric flow rate
Q_{out}	outgoing volumetric flow rate
v	fluid velocity
α	inclination of the axis of the radial ducts
Δp	pressure drop
ρ	fluid density
ζ	friction factor

Acronyms

CFD	Computational Fluid Dynamics
DCV	Directional Control Valve
FVM	Finite Volume Method
MRF	Multiple Reference Frame
PTO	Power Take-Off
VOF	Volume of Fluids

hybrid meshes were generated using Gambit®. A study on fluid flow in a high-speed rotating shaft with radial inlet using the finite volume method (FVM) is reported in [7], highlighting the impact of the supply pressure and the angular speed. Reference [8] investigates the effect of shaft speed, up to 2500 rpm, on the distribution of oil between two sets of radial outlets situated at varying distances from the inlet. In this case the FVM was used with Volume-of-Fluid method (VOF) for simulating the interfaces between the liquid and gaseous phases. For more extensive examinations of complex systems with rotating shafts, in [9] a lumped parameter model in Simcenter Amesim® of a high-performance engine lubrication system with the validation of the total inlet flow rate and the pressure in some points is reported. The 0D approach was also used in [10] for optimizing the flow rate distribution in a lubrication system of a heavy-duty tractor driveline and in [11] for the simulation of a 1.3 L engine lubrication circuit. Total flow rate and pressure in an engine lubricating circuit were also studied with Fluent in [12], while in [13] the flow distribution was evaluated by combining 1D and 3D fluid models, as well as multibody analysis. A combined 0D-3D simulation approach with VOF methodology was also used in [14] for studying the lubrication of a helical gear transmission and in [15] for the lubricant flow distribution in a wind power gearbox. The problem of evaluating the thermal losses in a gearbox can be also addressed using dedicated software packages, such as KISSsys®, that solve kinematics and heat transfer using analytic equations and data derived by ISO standard [16].

References [17] and [18] report the simulation of flow rates in a continuously variable speed hydrostatic transmission featuring multiple radial outlet ports. A comprehensive CFD simulation of the entire lubrication system of an internal combustion engine was carried out by different research groups with SimericsMP+® [19-21]. In all these last five studies, the FVM methodology was used.

Nevertheless, to the best authors' knowledge, limited emphasis has been placed on experimentally confirming the flow distribution within a rotating system featuring multiple outlet points. In [22] a numerical 0D model with experimental validation is proposed for studying the single-phase and two-phase flow through a rotating shaft with radial inlet and two radial outlets. As far as most complex circuits are concerned, in [23] the authors managed to measure the oil leaking through the roller bearings and gears coming from five different orifices by measuring the time to fill five separate boxed located underneath a vehicle transmission. The experimental data were used to validate a CFD particle-based Lattice Boltzmann technology model. In the recent paper [24], the flow through a rotating oil passage of a helicopter transmission system was studied. Authors validated the model developed in ANSYS Fluent based on FVM and VOF by means of a dedicated test bench for testing the shaft alone, with the possibility of measuring separately the flow rate at the two outlets by measuring the time for filling a volumetric burette. The comparison between simulated and experimental results are presented up to 1600 rpm, and the authors state an underestimation of the simulated flow rate above 800 rpm, with the error increasing with the speed. In their circuit the flow rate through the outlet closest to the inlet was always slightly higher than the flow in the next (farther) outlet.

This paper aims to fill this gap by contrasting, with experimental data, the results obtained from simulating a device equipped with three closely spaced sets of outlet holes within a shaft rotating at speeds of up to 5000 rpm. The primary objective of this study is to verify the accuracy of the Multiple Reference Frame (MRF) approach in simulating flow rate distribution by means of experimental measurements of the flow rates at all outlets. Moreover, the optimal setting of the CFD model and the accuracy of the lumped parameter approach are also assessed. This, in turn, would enable the methodology to be confidently employed in simulating various lubrication systems comprising both fixed and rotating components. This allows for optimizing the system in terms of energy efficiency, durability, and production costs. The structure of the paper is the following. In section 2 the experimental apparatus is described, while in section 3 the CFD model and its validation is presented; moreover, the influence of some geometric parameters on the flow rate distribution is analyzed. In section 4 the accuracy of a 0D approach is evaluated. Finally, in section 5 some guidelines emerged from the analysis carried out in paragraph 3 are applied to a portion of a real lubrication system.

2. Device for experimental tests

The system depicted in Fig. 1 was designed and manufactured [25] with the purpose of rigorously validating the simulation approach. It replicates the flow through a straight channel with three identical pairs of radial ducts at 180 degrees. The main characteristics include the possibility to adjust the angular speed of the shaft and accurately measure the flow rate through each outlet port. The shaft, mounted on ball bearings, is enclosed in a fixed steel cylindrical housing with an axial inlet and three outlet ports on the lateral surface connected to corresponding internal annular grooves. The housing is screwed on an interface block, while the shaft is driven by a variable speed electric motor. Elastic rings mounted on the outer surface of the shaft ensure effective sealing between the three annular groves, allowing the measurement of the flow rate contribution from the three rows of radial ducts. The driveline is capable of a maximum speed of 9000 rpm; however, for safety reasons, the maximum speed of the rotating device was limited to 5000 rpm.

The flow rate at the inlet port was generated by a hydraulic power unit consisting of a vane pump and a proportional load-sensing directional control valve (DCV) with maximum flow rate of approximately 40 L/min [26]. An integrated pressure compensator discharges the excess flow of the pump and maintains a constant pressure drop across the metering edges of the proportional valve. The inlet flow rate was measured using a gear flow meter (F1), VSE 1 GPO12V, with accuracy 0.3 % of the measured value and range 0.05 ÷ 80 L/min. The pressure at the inlet of the device was measured by a pressure gauge (PG), with resolution 0.05 bar and measuring range 0 ÷ 2.5 absolute bar (1 bar = 10^5 Pa). The circuit downstream from each outlet port had an identical layout and geometrical dimensions, with an internal cross section much larger than the cross section of the radial holes in the shaft, to generate a negligible, yet similar, resistance. Each circuit consisted of a branch of rigid pipe connected to a turbine flow meter (F2), KEM Küppers HM 11E, with range 6 ÷ 60 L/min, followed by a rubber hose ending in the

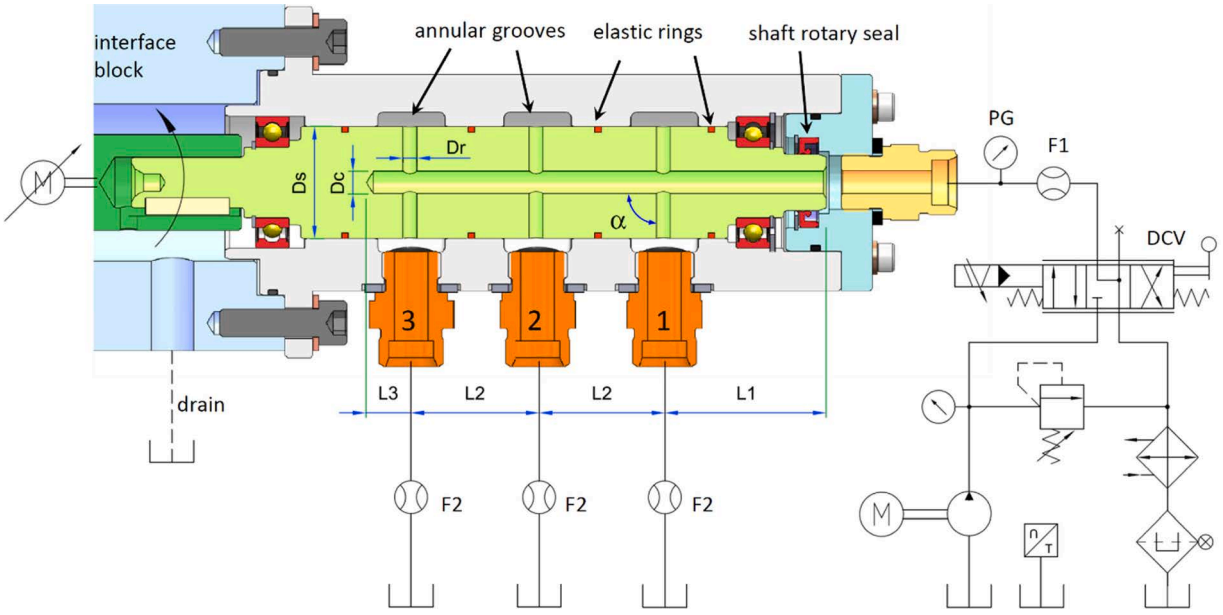

Fig. 1. Device for experimental tests and hydraulic circuit.

reservoir at atmospheric pressure. The linearity error of these instruments ranges between ±0.15 % and ±1 % of the instantaneous flow rate, depending on the Reynold's number and flowmeter size, while repeatability of the calibration curve is between 0.05 % and 0.1 %. A small leakage across the elastic rings is unavoidable; however, the oil leaking through the last ring and dropping through the vertical hole in the interface block was measured by means of a graduated burette. It was found that such leakage was three orders of magnitude smaller than the inlet flow rate, hence it was neglected. For the same reason, the leakages between the shaft and the housing were not considered in the CFD model. The tests were performed using a mineral oil with viscosity grade ISO VG46 at a temperature of 40 °C ± 2 °C. The oil temperature, measured by a PT100 sensor immersed in the reservoir, was controlled through a heat exchanger and an ON—OFF thermostatic valve mounted on the coolant line. The main geometric parameters of the mechanical device are reported in Table 1. A photo of the test rig, located at the Fluid Power Research Laboratory of the Politecnico di Torino, is shown in Fig. 2.

A NI data card was utilized to acquire the square wave signals from both the flow meters and the encoder on the shaft. The data were processed using a Virtual Instrument in Labview®. The tests were performed approximately 15 min after reaching the desired temperature. For each operating condition, the mean over 10 s intervals was computed.

3. CFD model

3.1. Model construction

The commercial software package ANSYS Fluent 2021 R1 was used for developing the CFD model employing the finite volume method. The fluid domain was partitioned into subregions to define different grid densities at the inlet, in the axial channel with radial holes, and in the three outlet pipes (Fig. 3). In general, two possible approaches can be considered for incorporating the rotation of the shaft: the use of rotating grids, which realistically simulate the movement of the shaft, or the modification of the equilibrium equations of the cells to virtually reproduce the force field resulting from angular velocity. A detailed description of these methodologies can be found in the review paper [27]. In this study, the latter approach, known as *Multiple Reference Frame* (MRF), was applied. In this manner, the entire mesh remains fixed, but different angular speeds can be imposed on each control volume. The technique is commonly used for the simulation of turbines [28], propellers [29], or wind turbines [30]. It represents a steady-state approximation, wherein the flow field is computed at a specific angular position of the shaft. The main advantage of this methodology is the significant reduction in computation time. In fact, it only requires a steady-state simulation, which is not time-dependent, whereas with rotating spatial meshes, it is necessary to run a dynamic simulation with an appropriate time step until a steady-state condition is reached. Moreover, the management of the sliding interfaces between the fixed and rotating meshes is less critical. A possible limitation is that the radial holes maintain the same position relative to the fixed ducts, whereas in reality this is not the case. However, it was verified that this simplifying assumption had no impact on the calculated results, as simulations performed with the shaft blocked at different angular positions showed no significant influence on the simulated flows. The final chosen position had the axes of the radial ducts coincident with the axes of the outlet holes, as illustrated in Fig. 3.

Table 1
Geometric parameters of the shaft.

Quantity	Value
Diameter Ds	40 mm
Diameter Dc	8 mm
Diameter Dr	5 mm
Length L1	58 mm
Length L2	45 mm
Length L3	13 mm
Angle α	90 deg

The tetrahedral mesh was generated using the ANSYS meshing tool. In the inlet and rotating pipe, the *body sizing* feature was applied to define a smaller size of the elements compared to the general mesh. Additionally, refinements were introduced in regions close to the connection surfaces between the rotating and stationary parts, using *contact sizing* features. Finally, the *program controlled* automatic inflation was applied to create five layers on the walls, and the *capture curvature* feature was activated (Fig. 4). A single-phase model of fluid with constant density and viscosity was used. No cavitation model was adopted since, in the considered operating conditions, no significant regions with negative gauge pressure were detected. Therefore, even if a model capable of simulating a multiphase fluid (with vapor or even air) had

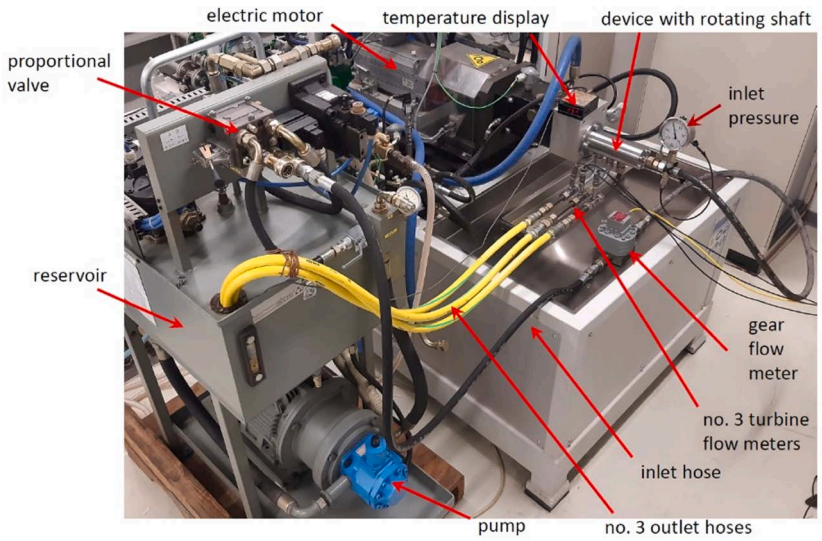

Fig. 2. View of the test rig with the hydraulic power unit on the left.

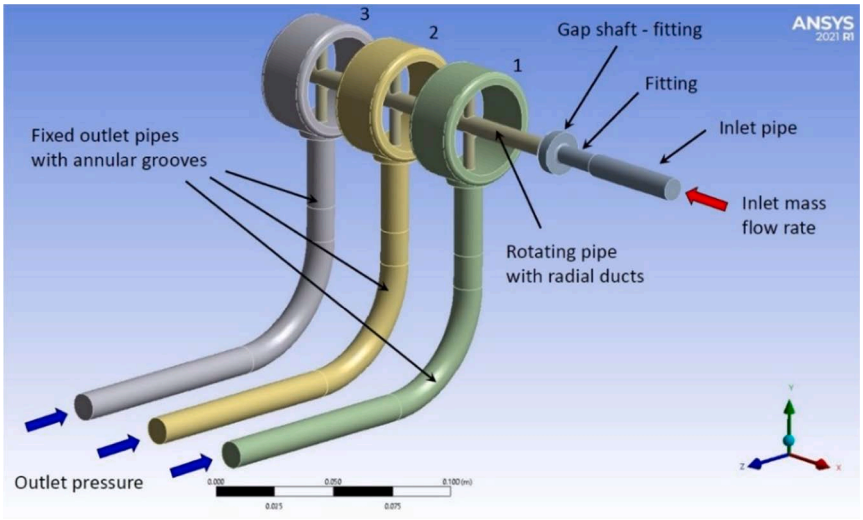

Fig. 3. Computational domains and boundary conditions.

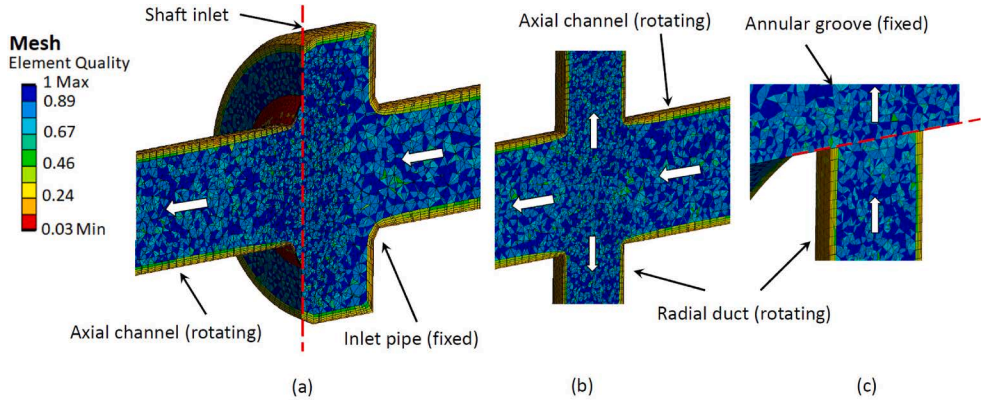

Fig. 4. Details of the mesh with about 2 million cells: (a) inlet of the rotating shaft, (b) intersection between the axial channel and a radial hole, (c) outlet of a radial hole.

been used, the computational domain would have been occupied only by the liquid phase.

Regarding the turbulence, although the k-ω model is usually suitable for the simulation of viscous fluids, a greater convergence difficulty was experienced with respect to the k-ε model. In fact, achieving the default residual of 10^{-3} on all quantities was possible only by using the 1st order

upwind discretization method for momentum, and the corresponding relaxation factor had to be reduced up to 0.3. In contrast, with the k-ε model it could be increased to 0.75 with a beneficial effect on computational time. On the other hand, the k-ε model is also commonly used in the simulation of volumetric machines, such as lobe [31] and spur gear pumps [32], that operate with speeds and fluids similar to those examined in the present study.

The final choice was the RNG k-ε model with *Enhanced Wall Treatment* as it allowed to get closer to the experimental results in the majority of analyzed cases, also consistent with a previous study [24]. This model is also suitable for working with Y^+ around 1, as in the case under examination. The 2nd order discretization scheme upwind for all equations (momentum, turbulent kinetic energy, and turbulent dissipation rate), except for PRESTO! used for the pressure, was adopted; the latter was chosen due to its faster convergence. Gradients were evaluated using the Green–Gauss Cell-Based method. Regarding the numerical scheme, the choice fell on *Coupled*. The SIMPLE scheme provides very similar results but with a number of iterations 3–4 times higher. Conversely, with the PISO scheme, the solution diverges.

As boundary conditions, mass flow rate at the inlet and atmospheric pressure at the three outlets were imposed. The simulations were performed under steady-state conditions.

3.2. Model optimization

The optimal balance between accuracy and computational time was determined through a mesh independence analysis. More specifically, an operating condition with a shaft angular speed of 5000 rpm and an inlet flow rate of 35 L/min was chosen as reference. Convergence conditions required achieving a residual of at least 10^{-3} for continuity, velocity, turbulence parameters (k and ε), as well as the quantities of interest, namely the three flow rates at the outlet and the supply pressure. The simulation ended when all conditions were satisfied simultaneously. In all cases, the variables that required the most iterations, and thus dictated the end of the simulation, were the flow rates at the three outlet ports. When the residual of 10^{-3} was reached for the flow rates, all other variables checked had residuals of at least the order of 10^{-4} if not even lower. In Table 2, the details of the cell size in the entire model and in the subregions with local refinement are reported. Five configurations were analyzed, with the number of cells ranging from approximately 600.000 to 8 million.

Fig. 5a illustrates the influence of the number of cells on the simulated flow rates, while in Fig. 5b the effects on the inlet pressure and computational time are shown. As observed, grid independent results were reached with approximately 2 million cells. The simulations were performed on a 24-core Intel Xeon Platinum 8268 processor with base speed 2.9 GHz using all physical cores. The actual speed during the simulations was around 3.4 GHz.

Table 2
Characteristic element size in the fluid regions for five models with different total number of cells.

Region	Element size (mm)				
	6E+5 cells	9E+5 cells	2E+6 cells	4E+6 cells	8E+6 cells
Base mesh	2.5	2	1.5	1.5	1.5
Inlet pipe (body sizing)	2	1	0.8	0.8	0.5
Rotating pipe (body sizing)	2	1	0.5	0.8	0.5
Inlet – Rotating pipe (contact sizing)	1	0.5	0.4	0.5	0.2
Rotating pipe - Outlet 1 (contact sizing)	1	0.5	0.4	0.2	0.09
Rotating pipe - Outlet 2 (contact sizing)	1	0.5	0.4	0.2	0.1
Rotating pipe - Outlet 3 (contact sizing)	1	0.5	0.4	0.2	0.1

The number of physical cores obviously has a significant impact on CPU time. However, as demonstrated in other studies [33], a sort of saturation is observed due to the excessive fragmentation of the computational domain (Fig. 6a). In this case, a slight worsening also occurs when all physical cores are used. Additionally, an increased difficulty in convergence is observed as the number of cores increases, since there is a progressive increment in iterations required to reach the same residual (Fig. 6b). On average, fixed shaft simulations require approximately only a fifth of the iterations compared to tests conducted at 5000 rpm.

3.3. Results and validation

The model was validated in terms of flow distribution through the three outlets and inlet pressure. For both experimental and simulated data, a verification of the consistency between the inlet flow rate Q_{in} and the sum of the outlet flows Q_{out} was performed. In the case of experimental data, utilizing data from the gear flow meter F1, a maximum discrepancy of 0.6 %, given by the Eq. (1), was found in the worst-case scenario. It is due to the measuring error of the transducers and the external leakages. The low error value confirms the reliability of the measured outlet flow rates.

$$error[\%] = \left| \frac{Q_{in} - \sum_{i=1}^{3} Q_{out,i}}{Q_{in}} \right| \cdot 100 \quad (1)$$

In the case of simulated data, the error was always lower than 0.02 %, and it is indicative of the model's good convergence.

Fig. 7 presents the model validation based on the flow rate distribution for two different total inlet flow rates in both cases with stationary and rotating shaft at 5000 rpm. In general, a strong correlation is evident between the simulated and experimental results, with the most significant difference observed for the percentage of the third row at 35 L/min and 5000 rpm. In the simulation it was 47.2 %, compared to 42.7 % in the experiment, corresponding to an overestimation of the calculated flow rate through that row of 1.57 L/min out of 35 L/min.

Clearly, both the experimental and simulated data reveal a significant increase in flow rate as the distance from the inlet point increases. Specifically, with a flow rate of 35 L/min, the flow through the last row of holes is twice that of the first row. This phenomenon is primarily attributed to the inertia of the flow and the negligible pressure drop caused by friction in the axial channel. This observation is substantiated by the fact that a slightly more uniform distribution is achieved when testing the stationary shaft with a lower inlet flow rate, corresponding to a lower fluid velocity at the inlet. In such cases, there is a higher flow through the first row and a lower flow through the third row compared to the test conducted at 35 L/min.

Regarding the influence of turbulence models, a comparison is made in Fig. 8. An evaluation based on a single operating condition is not reliable. In fact, it can be observed that all models yield the same results for the flow rate in the second row at 35 L/min, that the Spalart-Allmaras model appears to be the best for the flow rate in the first row at 15 L/min or that the RNG k-ε model with Standard Wall Function is more accurate in the third row at 35 L/min. However, considering also other cases not shown, overall, the best compromise can be achieved with RNG k-ε model with Enhanced Wall Treatment.

In Fig. 9a the difference in the fluid velocity profile between the inlets of the first and third radial ducts can be appreciated. In Fig. 9b the velocity along the Y axis as a function of the X-coordinate is shown for both radial ducts. It is evident that in the first channel the radial flow occurs mainly in the second half of the passage area (negative X values) leading to a lower vena contracta coefficient, while in the third one almost the entire duct cross section can be exploited. In both cases fluid recirculation is observed, being significantly higher in the first row.

In Fig. 10 the fluid velocity field is displayed using a cut plot on a

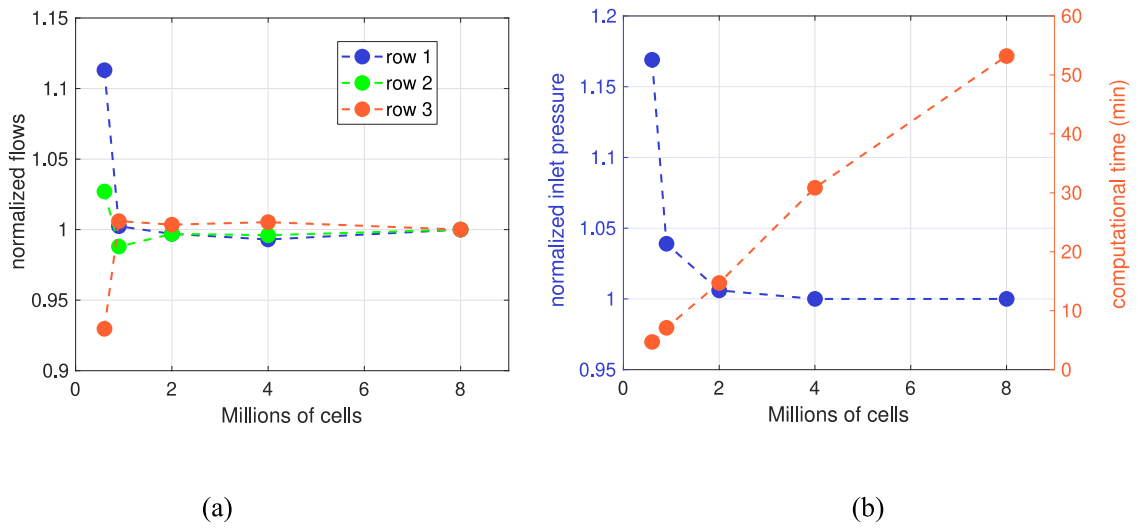

Fig. 5. Influence of the number of cells on the outlet flow rates (a), on the inlet pressure and on the computational time (b). Flow rate and pressure values normalized with respect to the case with 8 million cells.

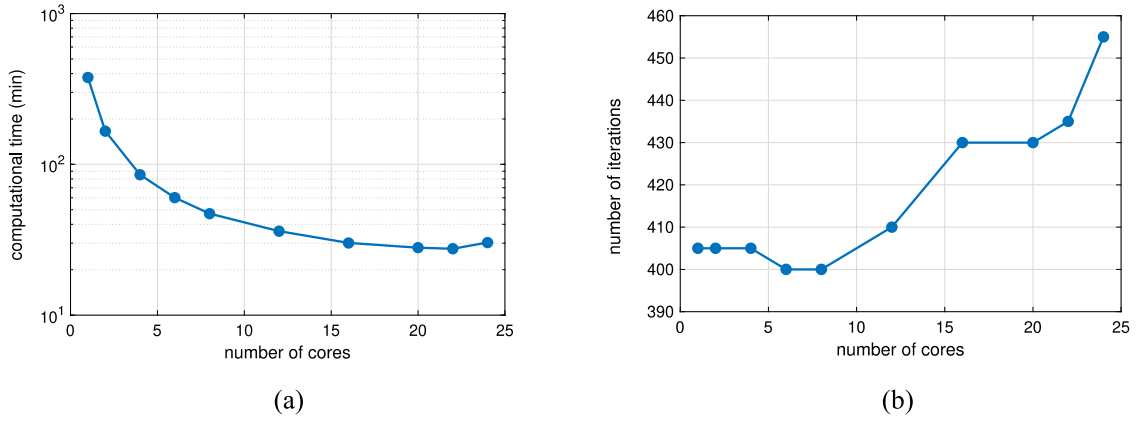

Fig. 6. Influence of the number of CPU physical cores on the computational time (a) and number of iterations (b) for the case at 5000 rpm and 35 L/min.

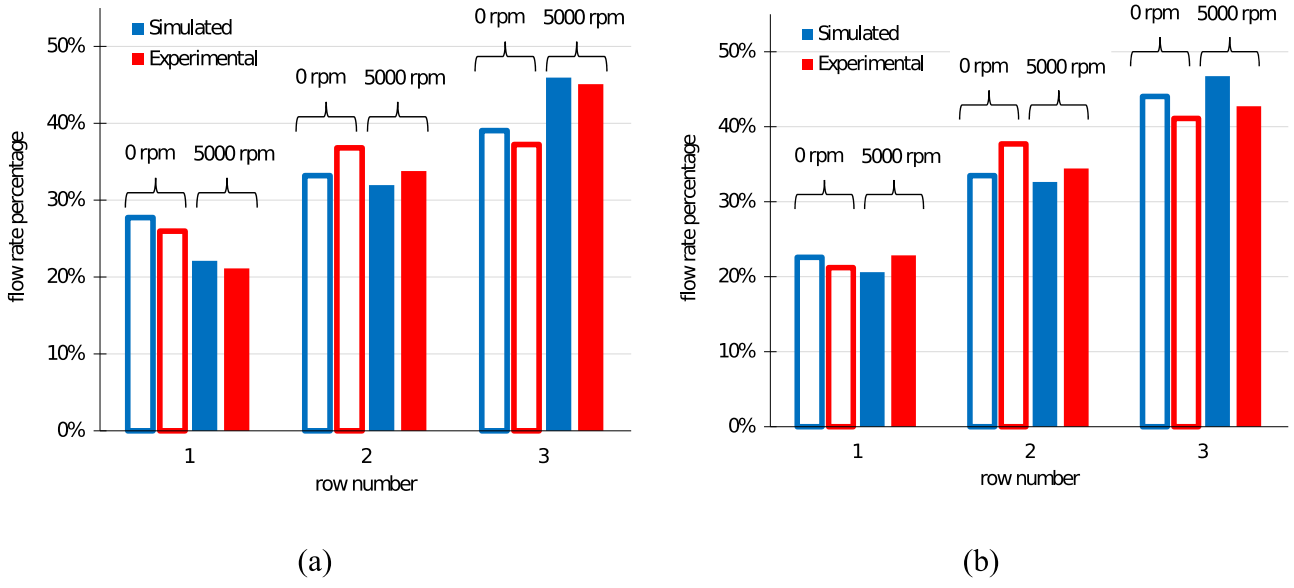

Fig. 7. Comparison between simulated and experimental distribution of the flow rates with total flow of 15 L/min (a) and 35 L/min (b).

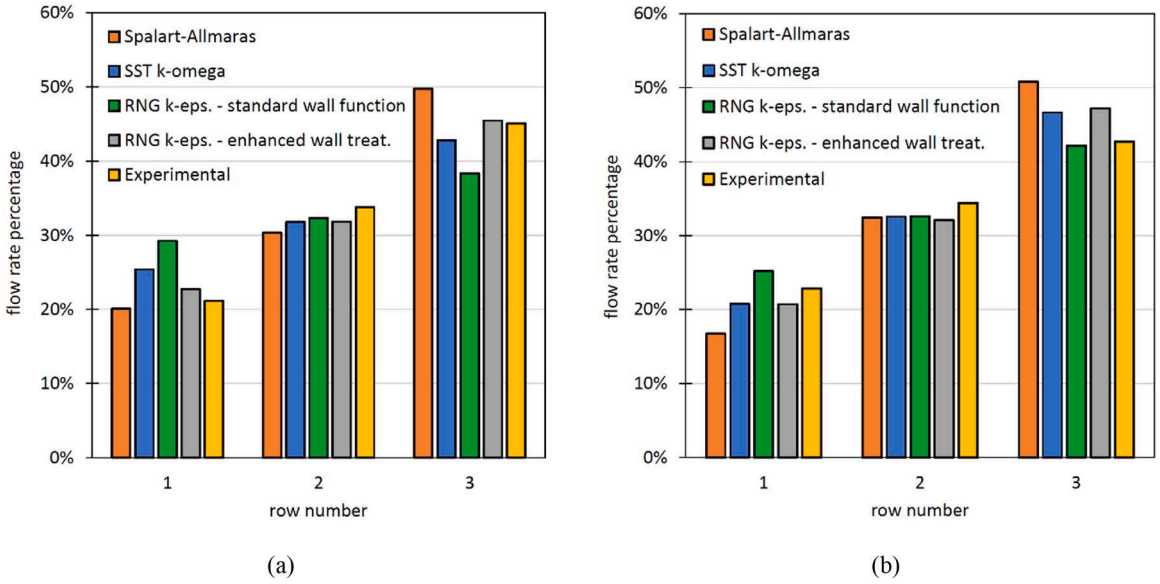

Fig. 8. Flow rate distribution with different turbulence models with angular speed 5000 rpm at 15 L/min (a) and 35 L/min (b).

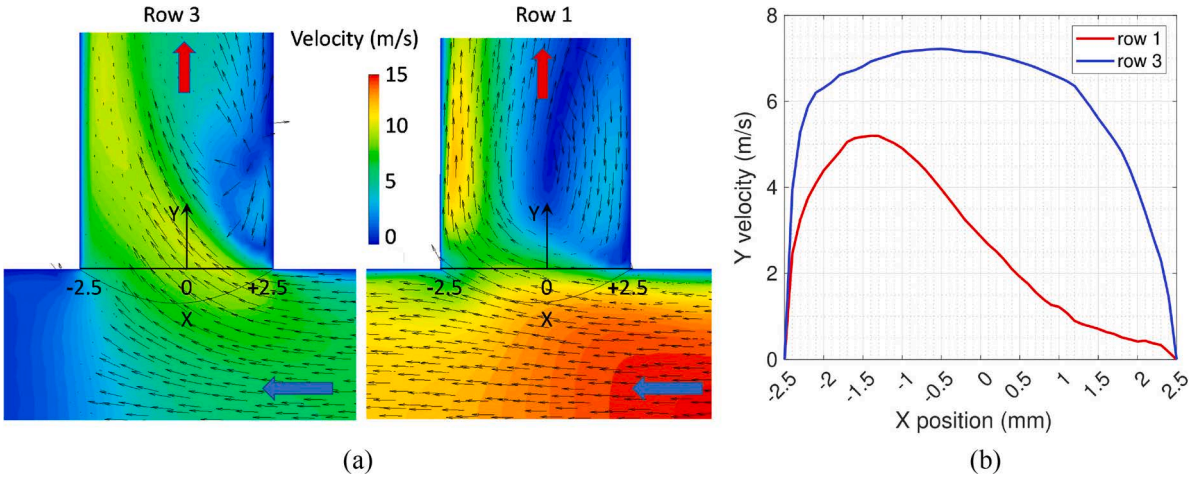

Fig. 9. Velocity profile at the inlet of radial channels 1 and 3 (a) and magnitude of the velocity along the Y axis as function of the position X (b). Condition with stationary shaft and 35 L/min.

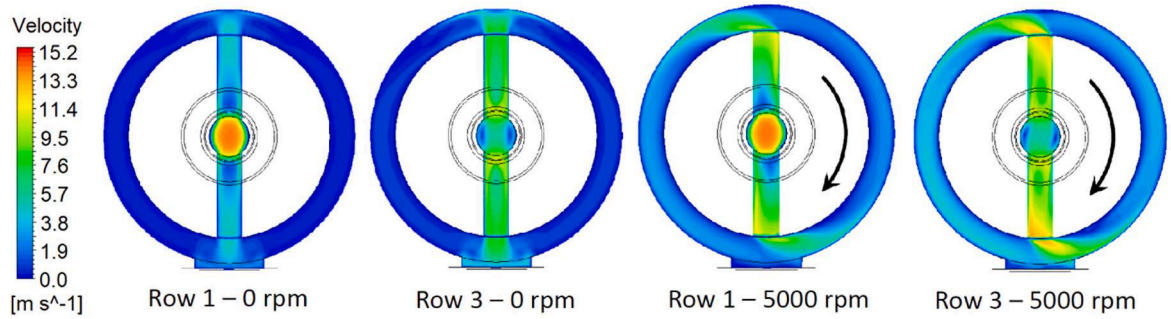

Fig. 10. Fluid velocity profiles in correspondence of the annular groove of the first and third row with inlet flow rate of 35 L/min.

plane perpendicular to the shaft axis, passing through the axis of the radial holes for different conditions. The effect of angular velocity can be observed, even though, as previously explained, the mesh is fixed in all fluid domains. In all cases, the velocity in the annular grooves is lower than in the radial ducts, indicating that the flow resistance is mainly dictated by the geometry of the shaft drillings. This confirms that the layout of the studied device is representative of a real lubricating system where annular grooves are not present.

In the case of a stationary shaft, the oil from the lower radial channel directly enters the outlet port, while the flow rate from the upper radial channel is divided equally. This means that the flow rate in the annular groove is one-fourth of the total inlet flow rate. In the case of a rotating

shaft, only a fraction of the flow rate leaving the lower duct enters directly the fixed outlet port, generating a higher flow rate in the annular groove. However, the velocity remains at least five times lower than in the channel. As mentioned earlier, both with the experimental apparatus and the model, a test was conducted with the stationary shaft rotated by 90 degrees, but no variation in the results was observed. This further confirms that the presence of the annular groove does not alter the flow inside the shaft. On the other hand, it was also verified that the pressure in the grooves practically coincides with the pressure at the inlet of the outlet pipes, as shown in Fig. 11.

It is interesting to note that from the inlet port and up to the first row of holes, the pressure decreases uniformly. After this point, an increase is observed at the inlet of the second section of the straight pipe, as well as at the inlet of the third section. The reason for this is that the flow rate in the axial channel suddenly decreases due to a fraction of the fluid flowing into the radial ducts. Consequently, the jet coming from the right hits the fluid region where the velocity is lower, generating a partial pressure recovery. At the bottom of the axial channel the pressure is similar to that at the inlet of the rotating shaft. It is clearly visible how across the last couple of radial ducts the pressure drop is significantly higher than across the holes of the first row.

The rotation of the shaft generates a sort of suction effect due to the centrifugal force on the oil in the radial ducts, leading to a decrease of the pressure in the axial channel. This pressure reduction could be considered as a positive effect since it also generates a reduction of the delivery pressure of the pump and a lower absorbed torque. However, a possible risk of low pressure in the axial channel is the separation of the air fraction if the pressure falls below the atmospheric value (gaseous cavitation). In the system under study, the most critical area is the recirculation zone at the inlet of the first radial ducts and then, progressively, in ducts 2 and 3. If the oil were also used for lubricating journal bearings, the load capacity of the bearing could be compromised by the presence of air bubbles. If the vapor pressure of the oil is reached (gaseous cavitation), the effect is a reduction of the oil flow rate starting from the first radial channel, which would make the flow distribution even more unbalanced. In fact, the inlet of the radial duct can be considered as an equivalent turbulent restrictor, where the flow rate is limited by the onset of the massive vapor cavitation [34,35]. In the case of the present model this condition is never reached for the angular speeds considered, therefore there was no need to activate the multiphase model.

In Fig. 12, the reduction of the pressure in correspondence of the inlet boundary condition, where the flow rate is imposed, is plotted as function of the shaft speed. The simulated points are perfectly interpolated by a 2nd order trendline, as the pressure reduction is proportional to the centrifugal force acting of the liquid volume in the radial ducts, that, in turn, is proportional to the square of the speed. Considering the typically low operating pressures of these systems and the fact that the tested device has a not excessively large shaft diameter with respect to other real applications, it can be understood how the rotational speed may play a crucial role in the pressure within the circuit.

3.4. Influence of geometric parameters on the flow distribution

The validation of the CFD model allows its confident use in studying the influence of various geometrical parameters. In more detail, the analyzed configurations were obtained by changing the following parameters one by one: the diameter of the axial channel D_C, the diameter of the radial holes D_R, the distance between the radial holes L2, and angle α of the radial holes with respect to the axis of the axial channel. It has just been observed that speed essentially influences pressure, while on the flow distribution, in the analyzed range between 0 and 5000 rpm, the effects are more limited. Moreover, the simulation time for the case at 5000 rpm is 5 times with respect to the case with stationary shaft. Therefore, only the results with stationary shaft are presented. It is essential to highlight that in some machines the pump is driven independently of the shaft with internal channels, so it is possible to have flow even with the shaft stationary, unlike in lubrication systems for internal combustion engines, where the pump is driven by the unique crankshaft. Hence simulating the flow rate with stationary shaft is a realistic condition. It is indisputable that once the model of a specific system is built, it can be used for obtaining the desired flow rate by selectively modifying the geometry of each hole. However, the focus here is to explore the possibility of finding general rules for initial rough sizing when aiming for a balanced flow rate distribution. In Fig. 13, the influence of diameters is reported. It can be noted that the most effective solutions involve increasing the diameters of the axial channel and reducing the diameter of the holes.

The reason can be explained by considering that the flow rate Q through each hole can be viewed as passing in a turbulent restriction, using the well-known Eq. (2):

$$Q = C_d \cdot A \cdot \sqrt{\frac{2\Delta p}{\rho}} \tag{2}$$

where C_d is the discharge coefficient, A the flow area, Δp the pressure drop and ρ the fluid density. Since all holes share the same downstream pressure, the pressure drop is solely a function of the upstream pressure in the junction. Moreover, the discharge coefficient, primarily influenced by the vena contracta coefficient, is affected by the local velocity in the axial direction, as depicted in Fig. 9a. The imbalance in flow rates in the reference system of Fig. 1 arises from the fact that the fluid velocity along the X-axis decreases from row 1 to row 3. Moreover, the static pressure increases, as demonstrated in Fig. 12. Consequently, the last row exhibits a higher discharge coefficient and a greater pressure drop compared to the first row. The increase of the diameter of the axial channel has the effect of reducing the fluid velocity along the X-axis, resulting in a smaller difference between the rows and limiting the pressure recovery at the end of the axial channel, thereby achieving a more uniform pressure distribution. In this way the difference between the flow rates is reduced. The reduction of the diameter of the radial holes has the effect of increasing the pressure throughout the axial channel, so the pressure recovery of a few tenths of bar has a lower

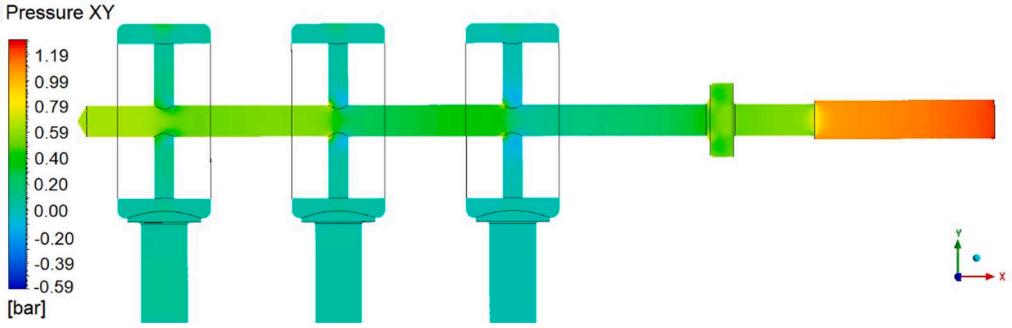

Fig. 11. Static gauge pressure distribution with stationary shaft and inlet flow rate 35 L/min.

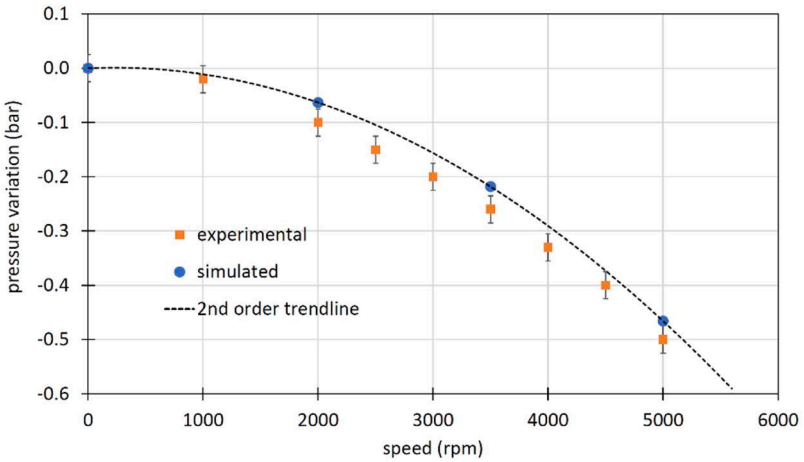

Fig. 12. Reduction of the inlet pressure vs. angular speed with inlet flow rate of 35 L/min.

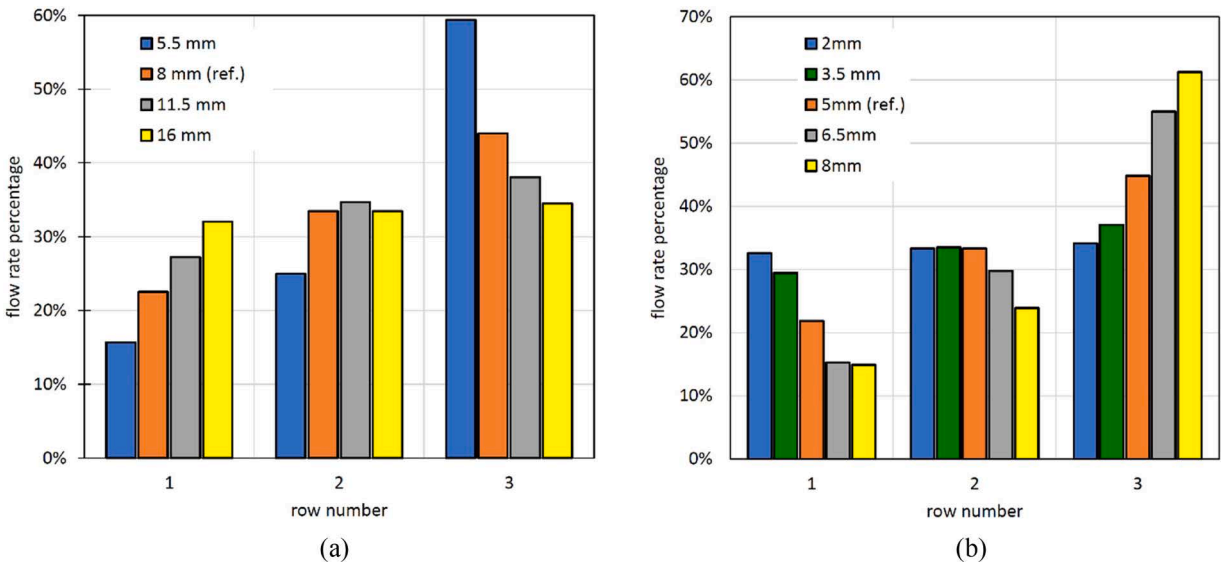

Fig. 13. Flow rate distribution with inlet flow rate 35 L/min and stationary shaft. (a) variation of the axial channel diameter D_C, (b) variation of the radial hole diameter D_R.

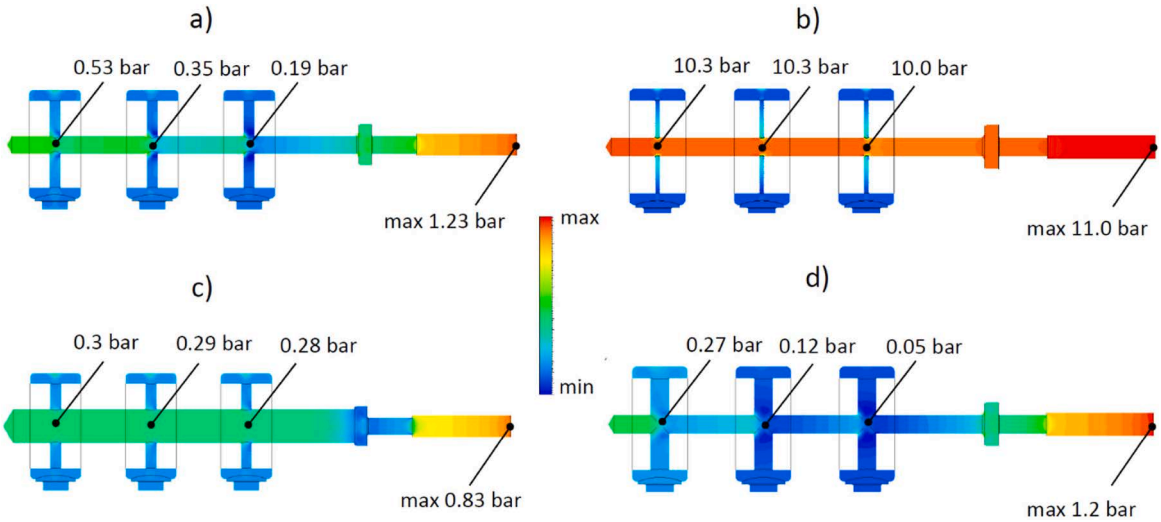

Fig. 14. Pressure field with inlet flow rate 35 L/min and stationary shaft for different geometric configurations: a) $D_C = 8$ mm, $D_R = 5$ mm; b) $D_C = 8$ mm, $D_R = 2$ mm; c) $D_C = 16$ mm, $D_R = 5$ mm; d) $D_C = 8$ mm, $D_R = 8$ mm.

relative weight and ensuring a similar pressure drop across the holes. In practice, a more uniform flow distribution is achieved when the dynamic pressure becomes smaller compared to the total pressure. The increase in pressure in the axial channel also has two further effects. On the positive side, when the shaft rotates at high speed, it avoids the risk of cavitation in the point where the minimum pressure is reached, namely before the first row (see Fig. 12). On the downside, it leads to greater power absorbed by the lubrication pump. In Fig. 14 the pressure field is shown for different configurations. It can be noticed that the layout with the most uniform flow distribution coincides with the layout with a limited percentage pressure variation between the three junctions. In the case with D_C= D_R= 8 mm, it is noteworthy that the pressure is slightly higher in the last annular groove than in the other two due to the significant flow rate imbalance. It means that in this case the model may underestimate the flow rate through the last row, and in the real case, where all radial holes have the same downstream pressure, the degree of imbalance could be even more pronounced.

The detail of the fluid velocity contours in the first and third junctions for the two configurations with the most homogeneous flow rate distribution is presented in Fig. 15. As mentioned earlier, since the simulations were conducted with the same inlet flow rate, the pressure levels differ due to changes in the geometry. It is evident that, contrary to the case reported in Fig. 9a, the two rows exhibit very similar velocity profiles indicating very similar flow rates.

In Fig. 16 the influence of the hole distance and inclination α with respect the shaft axis is reported. As the distance increases, the flow distribution becomes more homogeneous, with also the inversion of the trend in the simulation with L2 = 150 mm. This can be attributed to the increased distributed pressure drop in the pipe, which compensates for pressure recovery. It was found that a similar effect is generated by a significant increment of the fluid viscosity, i.e. the reduction of the operating temperature or the use of an oil with a greater viscosity grade. However, due to limitations in adjusting the temperature over a wide range in the test rig for quantitative validation, simulated results with high viscosity fluids are not presented.

Regarding inclination, its influence is minimal. However, a lower angle results in less deviation of the fluid stream, which helps the oil flow more easily through the first row.

The distance between rows is a parameter that the designer cannot freely adjust to modify the flow distribution, as the position of the radial holes is dictated by the location of the moving parts requiring lubrication. The distance can be high between the holes for lubricating gears or bearings located at the extremities of the shaft. Conversely, the lubrication holes for multidisc clutches must be positioned a short distance from each other, as in the reference system of Fig. 1, or even closer. Given this constraint, the only parameters available for adjustment are the diameters D_C and D_R. It is interesting to find a first attempt value of the diameter of the holes in relation to the diameter of the channel, which, in turn, will be a function of the total flow rate of the system. In Fig. 17 the flow distribution of all configurations analyzed in Fig. 13 is rearranged based on the ratio between the total flow area of the two radial holes in each row and the cross-sectional area of the axial channel. It can be observed that to maintain the flow rate through all rows within the range of 33 % ±5 % the area ratio must be quite small, with a threshold considered to be on the order of 0.4.

4. Lumped parameter model

Using the lumped parameter method, the circuit is simulated as a series of hydraulic resistances. This method, while simple and commonly used, does not always yield reliable results. The pressure drop Δp resulting from any resistance, such as a sudden restriction or expansion or a change in direction, is calculated with the Eq. (3):

$$\Delta p = \xi \cdot \rho \cdot \frac{v^2}{2} \tag{3}$$

where ζ is the friction factor, and v is the mean fluid velocity. The main limitation of this approach is that the coefficients remain valid only if each resistance is adequately separated from the others. In fact, these coefficients are measured under ideal conditions, where the resistance is placed in a sufficiently long, straight tube of constant diameter. Unfortunately, in engineering systems, this assumption is not always validated, and designers often overlook it.

Referring to a generic three-port junction in Fig. 18, the simplest approach for applying the Eq. (3) consists in using constant values of ζ, which are typically tabulated for various geometries and can be found in many technical manuals. With specific reference to T-junctions (α = 90 deg), literature often provides values for the friction factor of the flow coming from the main branch and deviating into the side branch ζ_{1-3}, ranging between 1.2÷1.5 [36,37], while, for the straight flow along the main branch, the friction factor ζ_{1-2} is typically around 0.1. However, the literature contains limited information on energy loss for the four-port cross-shaped junction case, with only one study available for circular cross-sections [38]. This lack of information also impacts the capability of computer software packages in simulating such geometries. Consequently, to exploit the potential of the state-of-the-art models already implemented in lumped parameter simulation software, geometry with a single radial hole for each row hole was simulated. To maintain the same flow area as the case with two holes, the diameter of

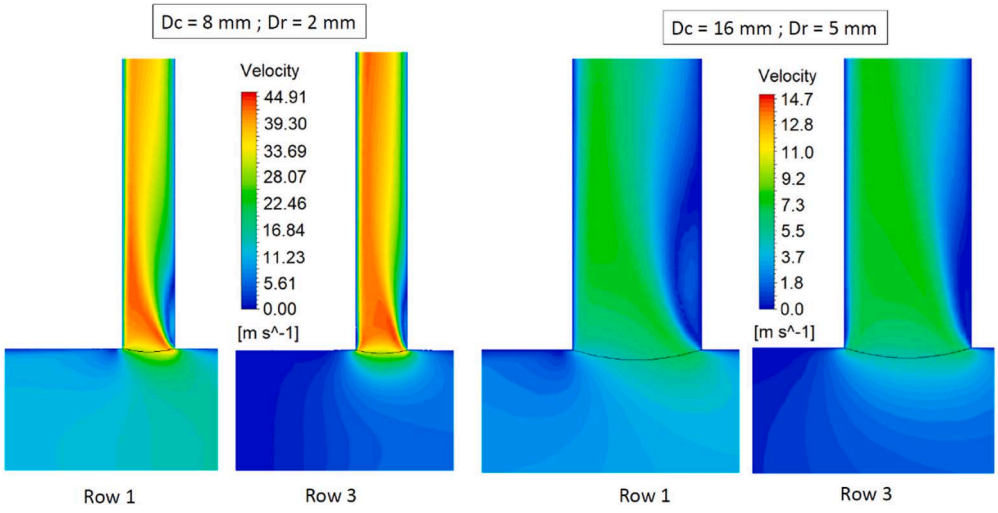

Fig. 15. Fluid velocity contours in the junctions of the first and third rows for two different geometric configurations.

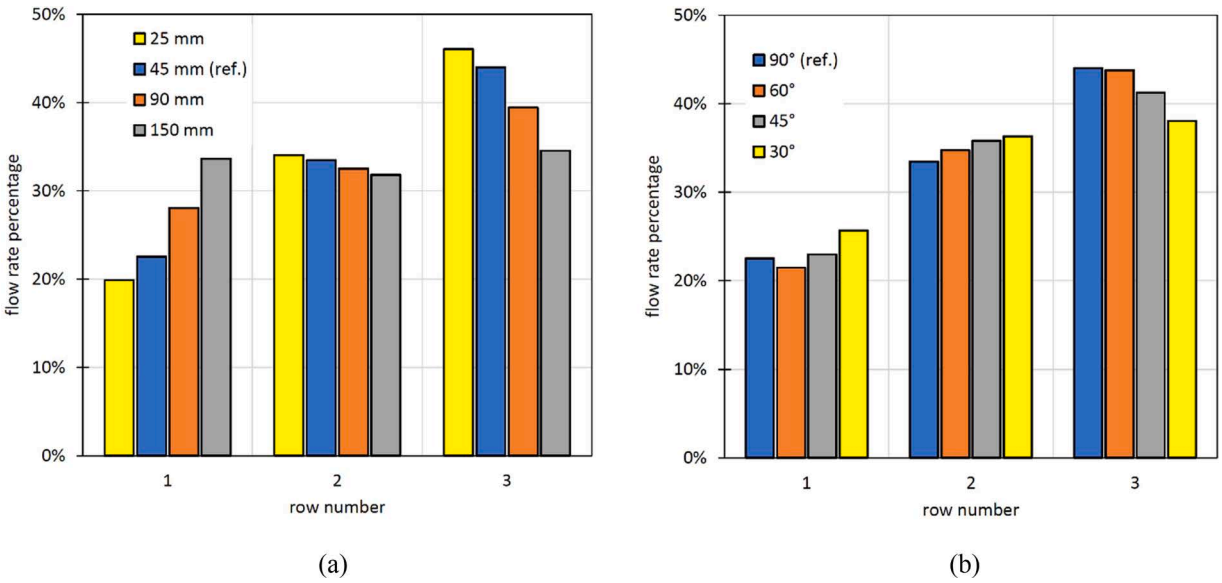

Fig. 16. Flow rate distribution with inlet flow rate 35 L/min and stationary shaft. Variation of the distance between the radial holes L2 (a), variation of the inclination of the radial holes (b).

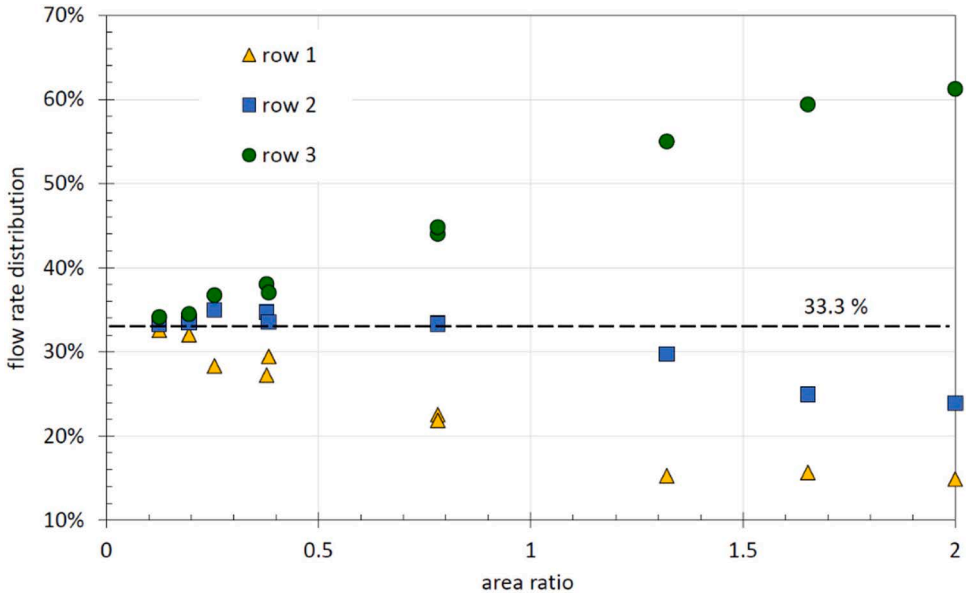

Fig. 17. Flow rate distribution as function of the ratio between the total flow area of the holes of each row and the cross section of the axial channel.

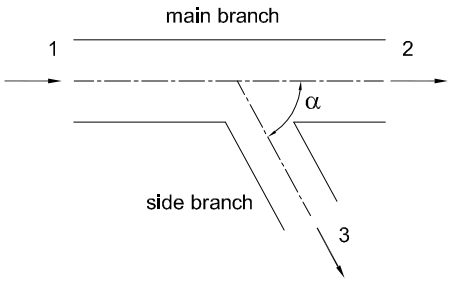

Fig. 18. Definition of the ports in a generic hydraulic junction.

the radial hole was increased from 5 mm to 7.1 mm. Although this hypothesis may seem quite daring and certainly introduces some approximations, for the purpose of calculating the flow distribution, the introduced error in this specific case is quite negligible, as demonstrated later.

A more accurate approach involves considering the friction factor not only as dependent on geometric parameters, but also as a function of the current operating conditions, such as fluid velocity and flow rates [39]. In this case the friction factor for the side branch is calculated with the Eq. (4):

$$\xi_{1-3} = A'\left[1 + \left(\frac{\nu_3}{\nu_1}\right)^2\right] \tag{4}$$

If the ratio between the cross sectional area of the lateral duct and the axial channel is greater than 0.35 and the ratio between the flow rates Q_3/Q_1 is lower than 0.6, as observed in the current case under study, the value of A' is determined by the expression (5):

$$A' = 1 - 0.6 \cdot \frac{Q_3}{Q_1} \tag{5}$$

The friction factor for the main branch is:

$$\xi_{1-2} = \tau \cdot \left(\frac{Q_3}{Q_1}\right)^2 \tag{6}$$

where:

$$\begin{aligned} \tau &= 2\left(2\cdot\frac{Q_3}{Q_1} - 1\right) \; if \; \frac{Q_3}{Q_1} \leq 0.5 \\ \tau &= 0.3\left(2\cdot\frac{Q_3}{Q_1} - 1\right) \; if \; \frac{Q_3}{Q_1} > 0.5 \end{aligned} \tag{7}$$

Both models, with variable and constant coefficients, were developed in the Simcenter Amesim environment, version 2304, using the Hydraulic Resistance Library. With reference to Fig. 19, the equations listed above are implemented in the submodels HR3P03, while the submodels HR230 simulate the pressure drop due to the first sudden restriction at the inlet of the hydraulic fitting, involving a reduction of diameter from 10 mm to 8 mm, and the second at the inlet of the shaft, entailing a change of diameter from 19 to 8 mm. For these last local resistances, the coefficients are calculated based on the formulation reported in [39] as well. The flow in the axial rotating pipes is simulated by the capacitive-resistive submodels HRL02A, while in the radial ducts by the submodels HRCE030, which also consider the centrifugal force. It was also verified that the use of 1D CFD models for simulating the pipes has no influence on results.

In the model with constant coefficients, the friction factors in the T-junctions were forced to be $\zeta_{1-3} = 1.5$ and $\zeta_{1-2} = 0.1$, while for the contractions, the values of 0.23 and 0.39 [36] were used respectively for the first and the second.

In Table 3, the values of the coefficients, calculated as function of the operating conditions for the case under study, are reported. Notably, it is observed that the friction factor ζ_{1-2} can assume slightly negative values. As explained in [39], the authors suggest that this phenomenon occurs due to a fraction of the slowly advancing low-velocity boundary layer near to the walls enters the side branch. This results in an increase in the energy per unit volume of the fluid in the straight passage compared to that in the side branch.

The results obtained from the lumped parameter models are presented in Fig. 20a in terms of flow distribution. The outcomes are compared with the simulation results of the CFD model with a single radial hole for each row with diameter of 7.1 mm. The experimental results are obviously relative to the original layout of Fig. 1 with two holes at 180 degrees; however, it has been verified using the CFD model that the variation of the number of radial holes at equal total flow area has minimal influence on flow distribution. This is depicted in Fig. 20b, where the case with four radial ducts per row at 90 degrees, each with diameter of 3.5 mm, is also reported.

In Fig. 21, the static pressure along the longitudinal axis is shown. As previously anticipated in Fig. 12, a pressure recovery is observed in the CFD model just after the location of the radial ducts. The 0D model with variable coefficient gives reasonably accurate results in terms of general trend, although it tends to overestimate the inlet pressure. This discrepancy may arise from the fact that the sudden expansion from 8 mm to 19 mm at the outlet of the fitting was not considered, given its proximity to the subsequent contraction. On the other hand, it was verified that the addition of this expansion results in an increase of the pressure losses of approximately 1 bar, leading to a significant overestimation of the circuit resistance. Paradoxically, with the 0D model with constant coefficients the same inlet pressure as the CFD model is obtained, although this appears more coincidental than systematically accurate.

Indeed, the analysis of the flow distribution in Fig. 20a leads to the conclusion that the constant coefficient model provides entirely inaccurate results. The variable coefficient model performs better since the flow rate in the second hole is computed quite well; however, the flow rate in the last row results being approximately six times that of the first row, whereas the evidence shows it to be only twice, as correctly predicted by the CFD model.

The reliability of the 0D model with variable coefficients increases as the diameter D_C of the axial channel and the distance L2 between the rows increase. This observation supports the notion that the formulation of the 0D model is valid only if there is no interaction between different local resistances. In fact, good results are obtained in the cases where the flow in the axial channel is minimally disturbed by the flow in the radial ducts, i.e., when the diameter D_C is significantly higher than the diameter D_R or, alternatively, when the distance L2 is at least 20 times D_C (Fig. 22).

Based on the results of this analysis, it is evident that the lumped parameter approach must be used very carefully if the aim of the study is the evaluation of the flow rate distribution. Moreover, since in a real rotating system it is impossible to validate or calibrate the model in terms of outlet flow rates, the evaluation of the model reliability based only on the measurable input quantities, i.e. pressure and total flow rate, would have led to the erroneous conclusion that the 0D constant coefficient model applied to the reference layout was sufficiently accurate and that the result on the flow rate distribution was also reliable.

5. Application to a real lubrication system

The simulation methodology was applied to the study of the lubricating system of a power divider installed on a fire truck. The function of the power divider is to redistribute the mechanical power from the internal combustion engine between the transmission shaft for vehicle traction and the PTO of the firefighting system. In Fig. 23 the shaft for driving the pump to supply the flow of firefighting fluid is shown. Lubricating oil enters the shaft axially coming from a fitting connected to the hydraulic circuit. The oil flows inside the axial channel of the shaft, reaching four bearings through three radial holes and the clutch disks through a total of 16 holes arranged in 4 rows. After exiting the shaft channels, the oil lubricates various internal components within the power divider housing (splash lubrication). Subsequently, due to gravity, it falls into the sump located beneath the assembly. For

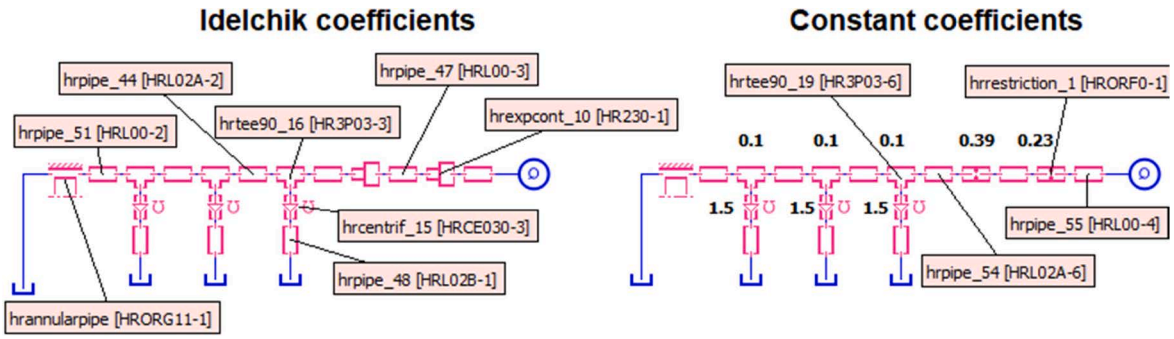

Fig. 19. Lumped parameter models in Simcenter Amesim.

Table 3
Coefficients calculated by the lumped parameter model based on reference [39].

1st restriction	2nd restriction	T-junction - row 1		T-junction - row 2		T-junction - row 3	
Inlet 10 mm	Inlet 19 mm	A' = 0.930		A' = 0.775		A' = 0.6	
Outlet 8 mm	Outlet 8 mm	$\tau = -1.531$		$\tau = -0.502$		$\tau = 0.3$	
ζ	ζ	ζ_{1-3}	ζ_{1-2}	ζ_{1-3}	ζ_{1-2}	ζ_{1-3}	ζ_{1-2}
0.189	0.439	0.953	−0.018	0.940	−0.073	1.567	0.3

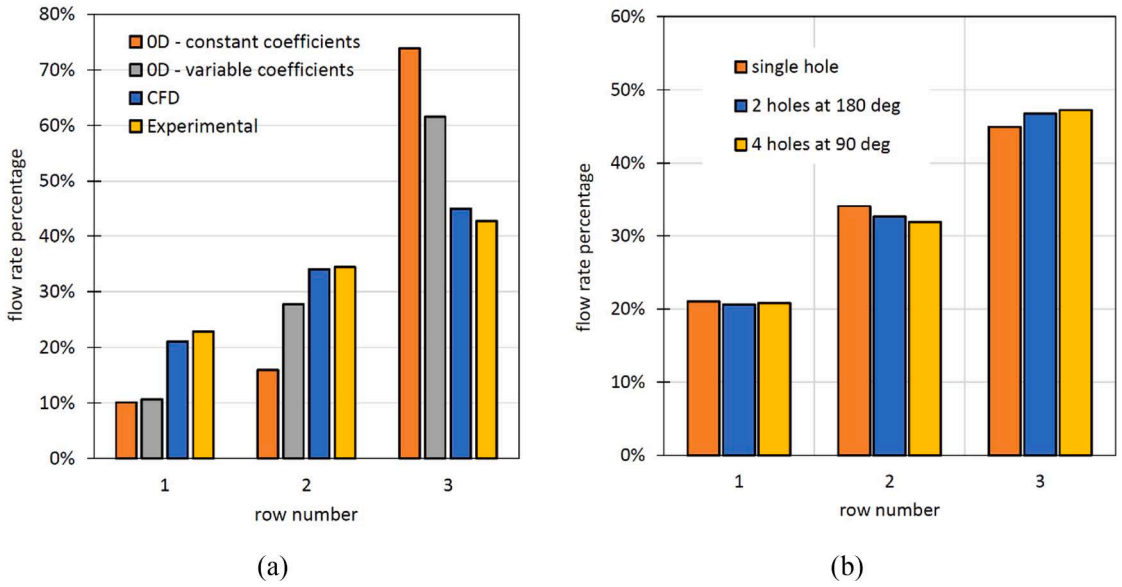

Fig. 20. (a) comparison between 0D and CFD models at 35 L/min and 5000 rpm; (b) influence of the number of radial channels per row at equal flow area simulated with the CFD model.

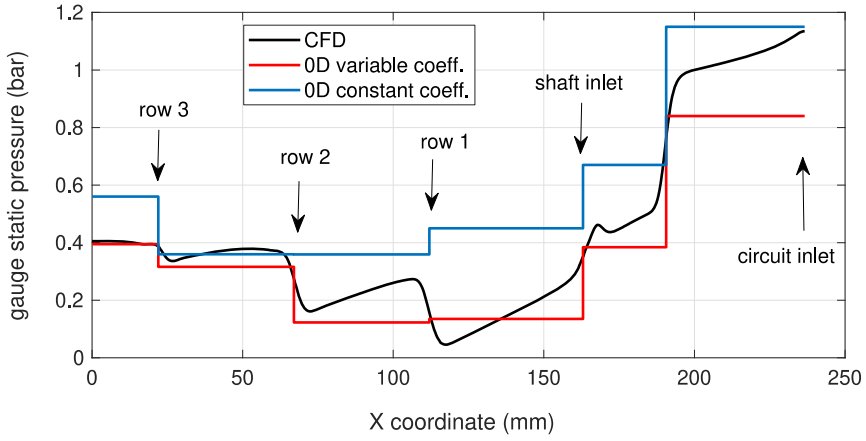

Fig. 21. Gauge static pressure in the axial pipe with inlet flow rate of 35 L/min and stationary shaft.

confidentiality reasons, the geometric parameters are not disclosed.

The aim is to verify the oil supply to the clutch ensuring proper lubrication of all disks. This involves evaluating the distribution of the flow rate through the four rows.

It is evident that, in this particular case, any type of experimental verification or data acquisition for calibrating a model is impossible. The limited spacing between the rows makes it unfeasible to measure the quantity of lubricant leaking from each rows using the method outlined in the paper [23]. Consequently, one must rely solely on the results produced by the model. Furthermore, the close proximity of the junctions inherently renders the assumptions for applying the lumped parameter model invalid from the beginning.

The fluid domain for the CFD model is shown in Fig. 24a. Similar to the system of Fig. 1, it includes a fixed grid in front of the shaft and the rotating ducts. In this case, the outlet boundary conditions are the atmospheric pressure imposed at the end of each radial hole, while a flow rate was imposed at the inlet. The mesh sensitivity analysis resulted in a grid with about four million cells, whose detail is reported in Fig. 24b. All other settings remained unchanged with respect to the three-row model.

Different geometric configurations were studied, with a specific focus on assessing the impact of the ratio *AR* between the total flow area of the radial holes of each row and the cross-sectional area of the axial channel:

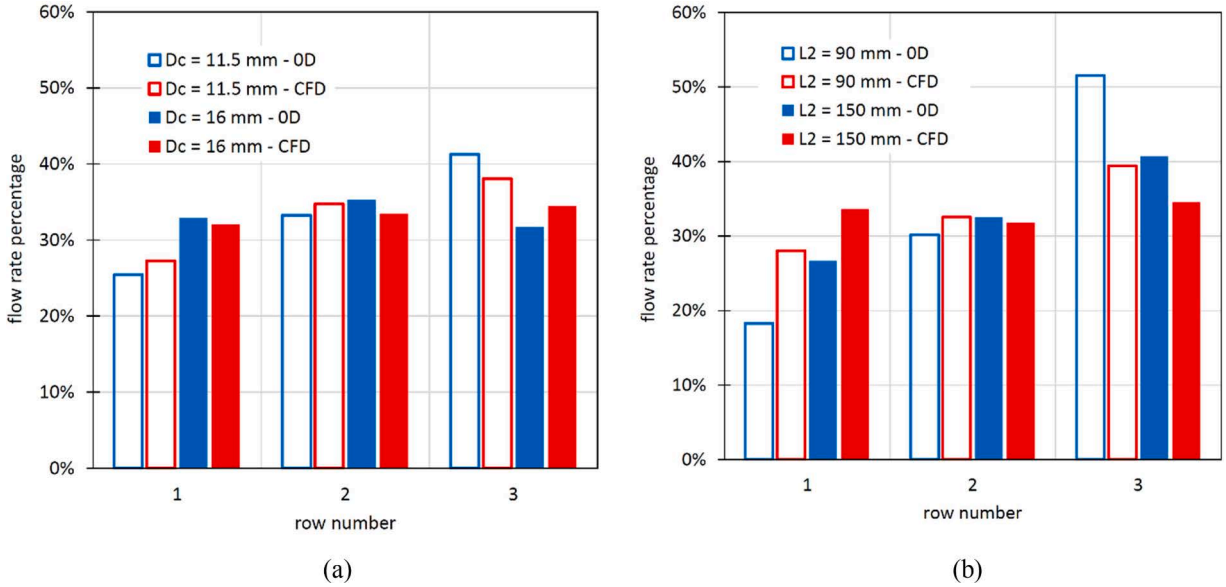

Fig. 22. Comparison between the CFD and the 0D model with variable coefficients and stationary shaft: (a) variation of the diameter of the axial channel, (b) variation of the distance between the rows.

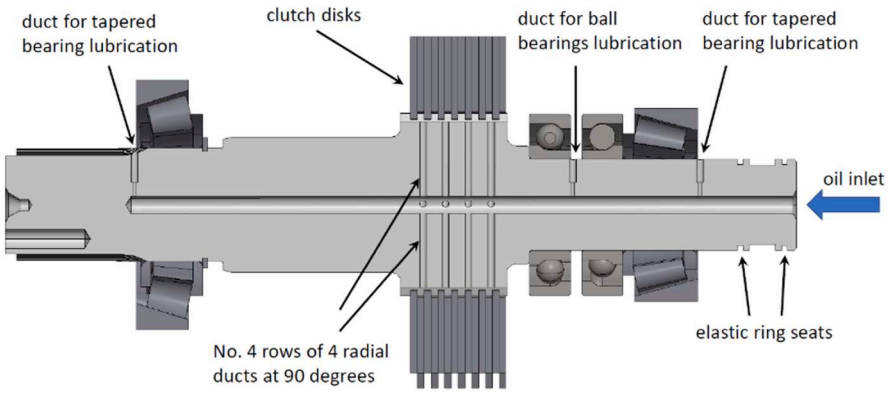

Fig. 23. Cross section of the shaft of the PTO for driving the pump of the firefighting system.

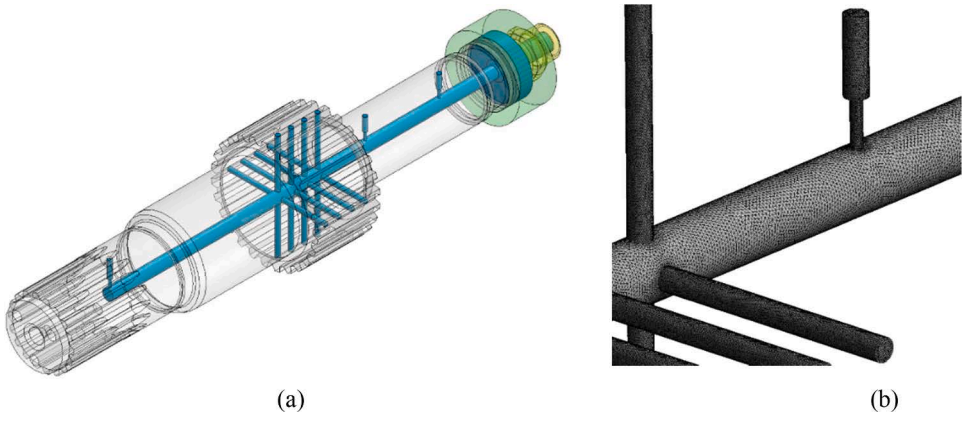

Fig. 24. (a) axonometric view of the computational domain, (b) detail of the mesh.

$$AR = \frac{\sum_{i=1}^{4} \frac{D_R^2}{4} R}{\frac{D_C^2}{4}\pi} = 4\frac{D_R^2}{D_C^2} \tag{8}$$

Fig. 25 illustrates the flow rate distribution, relative to the total flow for clutch lubrication, as a function of the area ratio. Also in this analysis, the influence of the rotating speed on the flow distribution was found to be minimal. Like the case of Fig. 1, a high value of the area ratio leads to a significant imbalance of the flow rate, with a serious risk of insufficient lubrication for the first clutch disk. It seems that an area

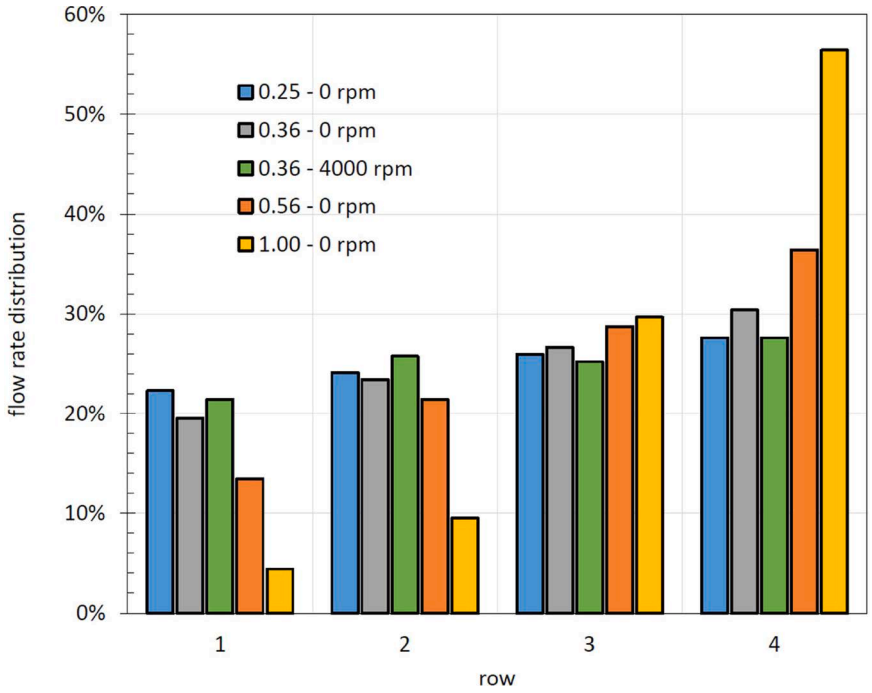

Fig. 25. Flow rate distribution through the four rows for different values of the area ratio.

ratio lower than approximately 0.4 is a good starting point for appropriately sizing the system, as obtained from the study on the three-hole shaft.

In Fig. 26, the velocity field is shown for the geometry with an area ratio equal to 0.56, representing a moderately unbalanced configuration. It can be noted that the longer distance from the fourth row and the bottom of the axial channel has no influence on the trend. Since the fluid beyond the fourth row is almost still, the oil is easily diverted towards the lateral ducts. Concerning the smaller holes for the lubrication of the roller bearings, the last one is the most favored, as it benefits from the pressure recovery in the final section of the axial channel. The second one is less favored, given the high axial velocity, causing the fluid to proceed in a straighter path. However, due to the distributed pressure drop along the axial channel, the first hole is more favored over the second due to a slightly higher pressure.

6. Conclusions

Previous research has extensively examined various layouts of lubrication circuits for internal combustion engines and mechanical transmissions. Simulations in these studies have been carried out with both 0D and 3D approaches. However, in almost none of these investigations, validation of flow rates at individual network outlets has been performed. In this paper, the CFD analysis of the flow through a rotating shaft with axial inlet and three couples of radial outlets has been contrasted with the experimental outcomes. It was found that the Multiple Reference Frame approach yields satisfactory results in terms of flow rate distribution and inlet pressure. The influence of the geometrical parameters has also been analyzed. Basically, to achieve a well-balanced distribution when dealing with junctions very close to each other, it is essential to make the local pressure recovery in the axial channel negligible with respect to the static pressure. This can be achieved in two different ways: by reducing the diameter of the outlets in order to increase the mean pressure level, or by increasing the diameter of the axial channel for lowering the axial velocity and, as a consequence, the recovery effect. The drawback of the former is a higher delivery pressure of the pump, while the disadvantage of the latter is a potential release of gaseous fraction when the shaft rotates. It has also been found that the classical lumped parameter approach is not reliable enough when the outlets are in close proximity. Better results are obtained in the case of low axial velocity or high distance between the junctions.

The obtained results provide best-practice guidelines for the correct simulation of similar systems, characterized by the impossibility of calibrating the model using experimental data, except for the input quantities to the circuit that, as demonstrated, are not sufficient to assess the reliability of the simulation. However, some unaddressed aspects are worth noting. Due to the limitation of the test rig, it has not been

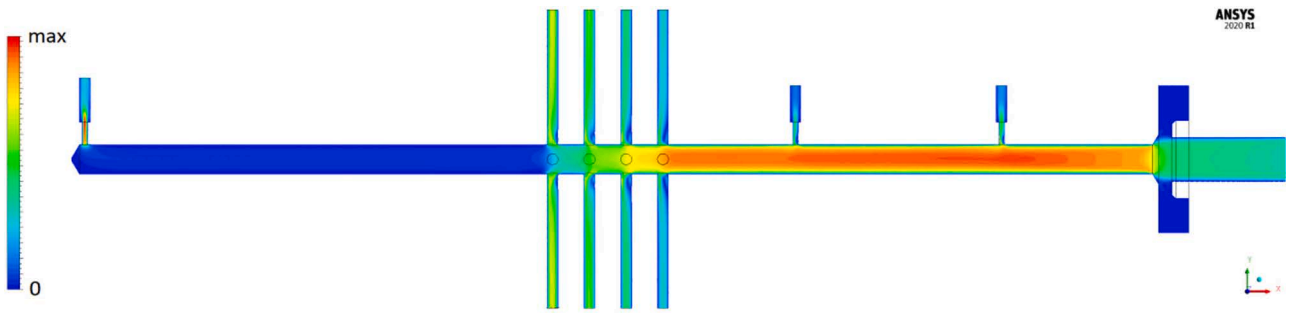

Fig. 26. Velocity distribution with area ratio equal to 0.56.

possible to check the methodology's reliability in harsher conditions, such as very high angular speed or low oil temperature. The former could lead to cavitation inside the shaft, necessitating consideration of a massive release of air. The latter implies high viscosity values, and a not negligible importance of the distributed pressure drops, whose influence on the flow distribution should be analyzed.

CRediT authorship contribution statement

Massimo Rundo: Writing – review & editing, Writing – original draft, Visualization, Validation, Supervision, Methodology, Formal analysis, Conceptualization. **Paola Fresia:** Visualization, Validation, Software, Methodology, Formal analysis. **Paolo Casoli:** Writing – review & editing, Conceptualization.

Declaration of competing interest

The authors declare that they have no known competing financial interests or personal relationships that could have appeared to influence the work reported in this paper.

Data availability

Data will be made available on request.

Acknowledgements

The authors acknowledge the support of Fresia SpA, Millesimo, Italy, for providing the CAD geometry of the lubrication system and for the contribution to the design of the experimental device.

Funding sources

This research did not receive any specific grant from funding agencies in the public, commercial, or not-for-profit sectors.

References

[1] B. Li, J. Hou, K. Xu, Optimal designs for flow uniformity at inlet of microchannel flat tube heat exchanger, Appl. Therm. Eng. 226 (2023) 120300, https://doi.org/10.1016/j.applthermaleng.2023.120300.
[2] F. Alnaimat, B. Mathew, Flow distribution in microchannel devices with U-shaped manifolds, Int. J. Thermofluids 19 (2023) 100391, https://doi.org/10.1016/j.ijft.2023.100391.
[3] J. Wang, Theory of flow distribution in manifolds, Chem. Eng. J. 168 (2011) 1331–1345, https://doi.org/10.1016/j.cej.2011.02.050.
[4] B. Zardin, G. Cillo, C.A. Rinaldini, et al., Pressure losses in hydraulic manifolds, Energies 10 (2017) 310, https://doi.org/10.3390/en10030310.
[5] P.G. Correa, J.R. Mac Intyre, J.M. Gomba, et al., Three-dimensional flow structures in X-shaped junctions: effect of the Reynolds number and crossing angle, Phys. Fluids 31 (4) (2019) 043606, https://doi.org/10.1063/1.5087641.
[6] Q. Yang, K. Liu, D. Zhu, et al., Optimizing pipe network of lubrication system for accurate oil distribution, in: Proceedings of the 7th International Conference on Fluid Power and Mechatronics, Harbin, China, 2015, https://doi.org/10.1109/FPM.2015.7337315. Aug. 5-7.
[7] Z. Xiong, W. Wu, S. Yuan, J. Hu, Investigation of the flow field inside an oil distribution mechanism at high speed, in: Proceedings of the 7th International Conference on Fluid Power and Mechatronics, Harbin, China, 2015, https://doi.org/10.1109/FPM.2015.7337077. Aug. 5-7.
[8] R. Sharma, V.K. Gupta, A. Khaware, V. Kamat, Efficient CFD methodology for optimal design of oil cooled electric motor shaft, J. Fluid Flow, Heat Mass Transf. 9 (2022) 66–75, https://doi.org/10.11159/jffhmt.2022.009.
[9] A. Senatore, M. Cardone, D. Buono, A. Dominici, Fluid-dynamic analysis of a high performance engine lubricant circuit, SAE Techn. Pap. (2007), https://doi.org/10.4271/2007-01-1963, 2007-01-1963.
[10] A. Polito, L. Montorsi, G. Muzzioli, et al., Numerical modeling of the critical operating conditions for a hydraulic lubrication system in a heavy-duty tractor driveline, SAE Techn. Pap. (2021), https://doi.org/10.4271/2021-01-1140, 2021-01-1140.
[11] A. Nain, Experimental and simulation analysis of 1.3 litre water cooled engine lubrication circuit, SAE Techn. Pap. (2022), https://doi.org/10.4271/2022-01-0182, 2022-01-0182.
[12] J. Gao, X. Gao, W. Zou, Three dimensional simulation of oil flow characteristics in lubrication system of rotary tillage engine, INMATEH-Agric. Eng. 65 (3) (2021), https://doi.org/10.35633/inmateh-65-17.
[13] H. Takagishi, Y. Ohtaka, K. Nemoto, et al., Establishment of engine lubrication oil pressure and flow rate distribution prediction technology using 3D-CFD and multi body dynamics, SAE Techn. Pap. (2009), https://doi.org/10.4271/2009-01-1349, 2009-01-1349.
[14] G. Muzzioli, G. Paini, F. Denti, et al., A lumped parameter and CFD combined approach for the lubrication analysis of a helical gear transmission, J. Phys.: Conf. Ser. 2385 (2022) 012034, https://doi.org/10.1088/1742-6596/2385/1/012034.
[15] J. Liu, Z. Xu, L. Zhang, J. Xiao, T. Tang, A lubricant flow distribution characteristic analysis of a wind power gearbox, Tribol. Int. 154 (2021), https://doi.org/10.1016/j.triboint.2020.106684.
[16] A.M. Teamah, M.S. Hamed, Numerical investigation of thermal losses within an internal gear train submerged in a multiphase flow and enclosed in a rotating casing, Int. J. Thermofluids 15 (2022), https://doi.org/10.1016/j.ijft.2022.100188.
[17] P. Marani, C. Ferrari, R. Paoluzzi, C. Stefano, Methods of computational fluid dynamics for a CVT transmission lubrication system of agricultural tractor, in: The 9th International Fluid Power Conference, Aachen, Germany, 2014. Mar. 24-26.
[18] C. Ferrari, P. Marani, K. Ghorpade, CFD modeling of lubrication system in agricultural power split transmission, in: 13th European Conference of the International Society for Terrain Vehicle Systems, Rome, Italy, 2015. Oct. 21-23.
[19] E. Frosina, A. Senatore, D. Buono, A tridimensional CFD analysis of the lubrication circuit of a non-road application diesel engine, SAE Techn. Pap. (2013), https://doi.org/10.4271/2013-24-0130, 2013-24-0130.
[20] S. Dhar, H. Afjeh, C. Srinivasan, et al., Transient, three dimensional CFD model of the complete engine lubrication system, SAE, Int. J. Engines 9 (3) (2016) 1854–1862, https://doi.org/10.4271/2016-01-1091.
[21] C. Srinivasan, S. Pasunurthi, R. Tawar, et al., Engineering applications of multi-dimensional CFD analysis of lubrication system, SAE Techn. Pap. (2020), https://doi.org/10.4271/2020-01-1110, 2020-01-1110.
[22] S.-W. Cheng, W.-J. Yang, Modeling of two-phase flow through a rotating tube with twin exit branches, Int. J. Rotating Mach. 6 (3) (2000) 159–166, https://doi.org/10.1155/S1023621X00000154.
[23] J. Li, Z. Ma, M. Jiang, et al., Optimized design of the flow network in the lubrication system for the heavy vehicle transmission, Adv. Mech. Eng. 9 (4) (2017) 1–16, https://doi.org/10.1177/1687814017696414.
[24] X. Hu, Z. Huang, A. Wang, The effect of rotating speed and oil supply pressure of the rotating passage of the transmission system for a helicopter, Tribol. Trans. 66 (5) (2023) 787–800, https://doi.org/10.1080/10402004.2023.2234429.
[25] P. Fresia, M. Rundo, Analysis of the flow rate through rotating shafts in lubricating circuits, in: 23rd Australasian Fluid Mechanics Conference, Sydney, Australia, 2022. Dec. 4-8ISSN: 2653-0597.
[26] A. Corvaglia, G. Altare, R. Finesso, M. Rundo, Computational fluid dynamics modelling of a load sensing proportional valve, in: Proceedings of the ASME-JSME-KSME 2019 8th Joint Fluids Engineering Conference, San Francisco, USA, 2019, https://doi.org/10.1115/ajkfluids2019-4708. July 29 – Aug. 1.
[27] L. Maccioni, F. Concli, Computational fluid dynamics applied to lubricated mechanical components: review of the approaches to simulate gears, bearings, and pumps, Appl. Sci. 10 (24) (2020) 8810, https://doi.org/10.3390/app10248810.
[28] A. Khedr, F. Castellani, Critical issues in the moving reference frame CFD simulation of small horizontal axis wind turbines, Energy Convers. Manag: X 22 (2024) 100551, https://doi.org/10.1016/j.ecmx.2024.100551.
[29] C. Hage, T. Sophy, E.H. Aglzim, A comprehensive study on the aerodynamic influence of stationary and moving obstacles on an isolated phantom DJI 3 UAV propeller, J. Eng. (2024) e12374, https://doi.org/10.1049/tje2.12374.
[30] M.H. Dao, Q.T. Le, X. Zhao, C.C. Ooi, L.T.P. Duong, N. Raghavan, Modelling of aero-mechanical response of wind turbine blade with damages by computational fluid dynamics, finite element analysis and Bayesian network, Renew. Energy 227 (2024) 120580, https://doi.org/10.1016/j.renene.2024.120580.
[31] D.K. Kanungo, R. Murmu, H. Sutar, A unique modelling strategy to dynamically simulate the performance of a lobe pump for industrial applications, Adv. Chem. Eng. Sci. 14 (2024) 57–73, https://doi.org/10.4236/aces.2024.142004.
[32] A. Mitov, N. Nikolov, K. Nedelchev, I. Kralov, CFD modeling and experimental validation of the flow processes of an external gear pump, Precesses 12 (2024) 261, https://doi.org/10.3390/pr12020261.
[33] B. Haddadi, C. Jordan, M. Harasek, Cost efficient CFD simulations: proper selection of domain partitioning strategies, Comput. Phys. Commun. 219 (2017) 121–134, https://doi.org/10.1016/j.cpc.2017.05.014.
[34] M. Martelli, S. Gessi, G.P. Massarotti, On peculiar flow characteristics in hydraulic orifices, in: Proceedings of the ASME/BATH 2017 Symposium on Fluid Power and Motion Control, Sarasota, USA, 2017, https://doi.org/10.1115/FPMC2017-4313. Oct. 16-19.
[35] P. Casoli, F. Scolari, M. Rundo, Modelling and validation of cavitating orifice flow in hydraulic systems, Sustainability 13 (13) (2021) 7239, https://doi.org/10.3390/su13137239.
[36] Aa. Vv, Manuale Dell'ingegnere Meccanico, Hoepli, Milan, Italy, 1994. ISBN:88-203-2080-0.
[37] E.M. Chaimovich, Automatismi Oleodinamici, 1978, Tecniche Nuove, Milan, Italy. ISBN: 88-85009-32-8.
[38] Z.B. Sharp, M.C. Johnson, S.L. Barfuss, W.J. Rahmeyer, Energy losses in cross junctions, J. Hydraul. Eng. 136 (1) (2010) 50–55, https://doi.org/10.1061/(ASCE)HY.1943-7900.0000126.
[39] I.E. Idelchik, Handbook of Hydraulic Resistance, Begell House Inc, New York, 2007, 4th Edition Revised and AugmentedISBN: 978-1-56700-251-5.